# Structure-function relation of the developing calyx of Held synapse *in vivo*

**Abbreviated title:** Strength-size relation of the calyx of Held

**Martijn C. Sierksma[1,3], Johan A. Slotman[2], Adriaan B. Houtsmuller[2] and J. Gerard G. Borst[1]**

[1]Department of Neuroscience or [2]Department of Pathology – Optical Imaging Centre, Erasmus MC, University Medical Center Rotterdam, 3000 CA, Rotterdam, The Netherlands.

[3]Sorbonne Université, Inserm, CNRS, Institut de la Vision, 17 Rue Moreau, F-75012 Paris, France.

Correspondence to g.borst@erasmusmc.nl

**Conflict of interest**: The authors declare no competing financial interests.

**Contributions**

JGGB and MCS designed experiments. MCS performed *in vivo* electrophysiology and imaging experiments, analyzed the electrophysiology and the images. JAS performed imaging experiments and imaging analysis. JAS and ABH designed imaging analysis. MCS drafted the manuscript. JAS, ABH and JGGB commented on manuscript.

**Acknowledgements**

This work was financially supported by the Earth and Life Sciences-Netherlands Organisation of Scientific Research (NWO, #823.02.006, 'Development of a Giant Synapse'). We are very grateful for the help of Elize Haasdijk and Celina Glimmerveen, who performed the immunolabeling. We thank Marcel van der Heijden, Peter Bremen and Aaron Wong for advice on the analyses.

**Abstract**

In adult rodents, a principal neuron in the medial nucleus of the trapezoid (MNTB) is generally contacted by a single, giant axosomatic terminal called the calyx of Held, but how this one-on-one relation is established is still unknown. Anatomical evidence suggests that during development principal neurons are innervated by multiple calyces, which may indicate calyceal competition, but *in vivo* electrophysiological recordings from principal neurons have indicated that only a single strong synaptic connection forms per cell. To test whether a mismatch between synaptic strength and terminal size exists, we compared strength of synaptic inputs during early postnatal development with the morphology of the synaptic terminals. *In vivo* whole-cell recordings of the MNTB neurons from newborn rats of either sex were made while stimulating their afferent axons, allowing us to identify multiple inputs. The strength of the strongest input increased to calyceal levels in a few days across cells, while the strength of the second strongest input was stable. Cells were subsequently immuno-labeled for vesicular glutamate transporters (VGluT) to reveal axosomatic terminals. Synaptic strength of the strongest input was correlated with the contact area of the largest VGluT cluster at the soma. No clear mismatch was observed between structure and strength. Together, our data agree with a developmental scheme in which one input strengthens and becomes the calyx of Held, but not with multi-calyceal competition.

**Significance**

Synapses are usually very small, but they can be as large as a cell body. What is the relation between the size of a synapse and its strength? We measured in neonatal rats the strength of a specific synaptic connection that grows in a few days from a small to a giant synapse, called the calyx of Held synapse. Synaptic strength was correlated with the contact surface of the largest glutamatergic terminal on the recorded neuron. Our results also suggest that during development only one of the

connections per cell increases in strength and expands over the soma, forming the calyx of Held synapse.

58 **Introduction**

59 Synapses come in a large variety of sizes and shapes. Most terminals have a diameter of about one
60 µm, forming a single synaptic contact on a dendrite. In contrast, some synaptic terminals are >10
61 µm, and contain >100 release sites (Atwood & Karunanithi, 2002; Rollenhagen & Lübke, 2006). These
62 large synapses have facilitated the study of the biophysical properties of synapses. A prime example
63 is the calyx of Held synapse in the auditory brainstem. The calyx spans ~20 µm, large enough to be
64 accessible for patch-clamp electrophysiology (Forsythe, 1994; Borst *et al.*, 1995). Owing to the
65 presence of hundreds of active zones (Sätzler *et al.*, 2002; Taschenberger *et al.*, 2002; Dondzillo *et*
66 *al.*, 2010), the calyx of Held can rapidly trigger action potentials in its target, a glycinergic neuron in
67 the medial nucleus of the trapezoid body (MNTB), thus functioning as a fast, high-fidelity, inverting
68 relay in the auditory brainstem (Borst & Soria van Hoeve, 2012).

69 The calyx of Held synapse grows from an axon of a globular bushy cell (GBC) that will initially form
70 small boutons. In rodents these contacts appear before birth (Kandler & Friauf, 1993; Hoffpauir *et*
71 *al.*, 2006; Rodríguez-Contreras *et al.*, 2008; Hoffpauir *et al.*, 2010; Holcomb *et al.*, 2013). Although
72 the innervation initially is highly divergent, eventually a GBC will give rise to only one or a few
73 calyces, and most adult principal neurons are innervated by a single calyx of Held (Held, 1893;
74 Morest, 1968; Kuwabara *et al.*, 1991; Kandler & Friauf, 1993; Rodríguez-Contreras *et al.*, 2006). The
75 developmental mechanisms that ensure the transition to the one-on-one innervation are largely
76 unclear (Yu & Goodrich, 2014). This transition happens between the second and the fifth postnatal
77 day (P2-5). At P5 the strength of one input overshadows the other ones (Chuhma & Ohmori, 1998;
78 Hoffpauir *et al.*, 2006; Hoffpauir *et al.*, 2010; Sierksma *et al.*, 2016), and one of the terminals has
79 expanded over the soma of the neuron (Hoffpauir *et al.*, 2006; Holcomb *et al.*, 2013). From these
80 studies it was suggested that half of the MNTB neurons are contacted by multiple calyces at this age
81 range (Hoffpauir *et al.*, 2010; Holcomb *et al.*, 2013), in agreement with observations from mouse
82 slice recordings (Bergsman *et al.*, 2004; Hoffpauir *et al.*, 2010; Xiao *et al.*, 2013). However, *in vivo*

83 physiological evidence for calyceal competition was observed in only very few cases for the rat
84 (Sierksma *et al.*, 2016).

85 These findings may indicate a discrepancy between terminal size and synaptic strength. To test this
86 possibility, one needs to correlate synaptic structures with synaptic strength. Serial sectioning of
87 tissue combined with EM offers the possibility of fully reconstructing every synapse in a restricted
88 volume (Denk & Horstmann, 2004; Hoffpauir *et al.*, 2006; Holcomb *et al.*, 2013), and allows the
89 reconstruction of entire calyces (Sätzler *et al.*, 2002; Holcomb *et al.*, 2013; Qiu *et al.*, 2015).
90 However, it does not offer a direct estimate of synaptic strength. Whereas slice electrophysiology
91 has the advantage of allowing simultaneous recordings of pre- and postsynaptic structures (Borst *et*
92 *al.*, 1995; Rodríguez-Contreras *et al.*, 2008), there is the uncertainty associated with possible cutting
93 of inputs during slice preparation. Immunolabeling of vesicular glutamate transporters (VGluT)
94 localizes synapses in the MNTB (Rodríguez-Contreras *et al.*, 2006; Rodríguez-Contreras *et al.*, 2008;
95 Soria Van Hoeve & Borst, 2010). As Piccolo, an active zone protein (Südhof, 2012; Gundelfinger *et al.*,
96 2016), is present in young calyces (Dondzillo *et al.*, 2010), the combination of VGluT and Piccolo may
97 indicate synaptic connectivity in the MNTB. How VGluT relates to synaptic strength is still unclear.
98 We therefore combined VGluT immunolabeling with *in vivo* whole-cell recordings during which we
99 recorded the inputs that are regularly active (Lorteije *et al.*, 2009; Sierksma *et al.*, 2016). We applied
100 electrical stimulation of the afferent axons to further identify the developing inputs. The recorded
101 cells were subsequently immunolabeled for VGluT and Piccolo, allowing a direct comparison
102 between synapse strength and structure for the developing calyx of Held synapse.

## Materials & methods

### *Animals*

All procedures conformed to the European legislation and were approved by the local animal ethics committee (EDC, project no. 115-14-11). Wistar dams (WU) were purchased from Charles River and housed within the Erasmus animal facility (EDC). The day of birth or finding the litter was taken as postnatal day (P)0. The dams had *ad libitum* access to food and water, and additional bedding and shelter material was provided for nest building.

### *Surgery and in vivo electrophysiology*

We used a ventral approach to gain access to the auditory brainstem, as described previously (Rodríguez-Contreras *et al.*, 2008; Sierksma *et al.*, 2016). First, we searched for bursting activity with a glass electrode to find the presumed location of the MNTB. When bursting activity was found, the search pipette was retracted and a bipolar stimulation electrode (MicroProbes for Life Science, PI2ST30.1H10) was placed contralateral from the recorded MNTB, straddling the trapezoid body, as described by Crins *et al.* (2011). Successful placement was assessed by measuring the stimulation current threshold and size of the field potential.

Whole-cell recordings with biocytin (2 mg/mL) in the pipette solution were made from principal cells; to be confident that the recording was obtained from the same neuron as the one that was recovered with immunolabeling, we made whole-cell recordings from only a single principal neuron per animal. Whenever a glia cell or non-principal cell was encountered, the pipette was retracted and a new pipette was used. Membrane potentials were compensated prior to the recordings for a liquid junction potential of -11 mV. Drift in membrane potential was <5 mV and remained uncorrected. Recordings were made with a MultiClamp 700B in current-clamp mode, with bridge balance set in the range of 20-70 MΩ and pipette capacitance compensation ~4-6 pF. Signals were low-pass filtered with a 4-pole Bessel filter at 10 kHz and digitized by a DigiData 1440A (Molecular Devices Co.) at 25 kHz. Acquisition was done with Clampex 10.2 running on a Windows XP computer.

128 Stimulation intensities were manually adjusted during the experiments. First, we quickly assessed at
129 which stimulation levels new excitatory postsynaptic potentials (EPSPs) were recruited, and at which
130 polarity most inputs could be discerned. Then, stimulation intensity was lowered to the activation
131 threshold of the first input, and step-wise increased over time. In some experiments the stimulation
132 intensity was also stepwise reduced, and then the data were pooled. For every stimulation strength
133 >30 sweeps were collected at 2 Hz. Stimulation current was typically below 0.4 mA to prevent
134 damage to the axons; at high stimulation currents (0.3 mA or higher) antidromic APs with latencies
135 <1 ms were often elicited in the principal neuron. This could still happen even though we used
136 bipolar stimulation electrodes, placed on the contralateral side from the recorded neuron.
137 Preferably, the stimulation electrode would be placed at the midline, where all calycigenic axons
138 converge ventrally. However, to avoid direct postsynaptic activation we placed the stimulation
139 electrode more laterally. This location may have led to preferential activation of the axon bundles
140 that run ventrally from the other MNTB (Kandler & Friauf, 1993).

141 After a recording the animal was deeply anesthetized and perfused with 6-10 mL of cold saline (0.9%
142 NaCl, w/v), followed by 8-10 mL of 4% of paraformaldehyde (PFA, w/v) dissolved in 0.12 M
143 phosphate-buffer (PB, pH 7.2-7.4).

144 ***Antibodies***

145 The following primary antibodies were used: rabbit polyclonal anti-Piccolo (Synaptic Systems
146 142003, RRID: AB_2160182; 1:1000), guinea-pig polyclonal anti-vesicular glutamate transporter 1
147 (Millipore AB5905, RRID: AB_2301751; 1:3000) and 2 (Millipore AB2251, RRID: AB_1587626;
148 1:3000). Secondary antibodies Alexa Fluor 488 against rabbit and Alexa Fluor 645 against guinea pig
149 were obtained from Jackson (1:200 or 1:400). Streptavidin-Alexa Fluor 594 conjugate (1:200) was
150 obtained from Thermo Fisher Scientific. Throughout, VGluT labeling refers to both VGluT1 and
151 VGluT2.

152 ***Immunolabeling procedure***

153 Immunolabeling procedure was based on the free-floating method. After perfusion the brain was
154 carefully removed from the skull, and post-fixed overnight at 4 °C. Then, it was left overnight in 10%
155 (w/v) sucrose in 0.1 M PB, embedded in 10% (w/v) gelatin and 10% (w/v) sucrose, and again fixed
156 overnight at 4 °C in 30% (w/v) sucrose and 10% (w/v) formaldehyde. The brain was cryoprotected
157 with 30% (w/v) sucrose solution in 0.1 M PB for >24 hr at 4 °C. Coronal slices (40 µm) were made on
158 a freezing microtome, and were collected in 0.1 M PB. The sections were heated for 3 hr to 80 °C in
159 10 mM sodium citrate (pH 6 at RT), washed four times for 10 min with 0.9% (w/v) NaCl in 0.05 M PB
160 (PBS). Then, the sections were pre-absorbed for 1 hr at RT with 10% (v/v) normal horse serum and
161 10% (v/v) Triton X-100 in PBS followed by 36-48 hr incubation under gentle agitation at 4 °C with
162 primary antibody solution containing 2% (v/v) normal horse serum, 0.4% (v/v) Triton X-100 and the
163 primary antibodies. The slices were washed four times for 10 min in PBS at RT, and incubated for 2
164 hr under gentle agitation at RT in the secondary antibody solution containing 2% (v/v) normal horse
165 serum, 0.4% (v/v) Triton X-100, and the secondary antibodies. For the biocytin-filled cells the
166 streptavidin conjugate was also added at this step. The slices were washed once for 10 min at RT
167 with PBS, and incubated for 10 min RT in 0.3 µM DAPI (D3571, Invitrogen) in 0.1 M PB. Sections were
168 then washed three times at RT with 0.1 M PB, mounted on glass coverslips with gelatin-chrome
169 alum, air-dried, and closed with Mowiol mounting solution containing 10% (w/v) Mowiol 4-88, 25%
170 (v/v) glycerol in 0.1 M Tris-buffer (pH 8.5). Sections were kept at 4 °C in the dark until further use.

171 ***Confocal and structured illumination imaging***

172 Confocal imaging was done on a Zeiss LSM 700 microscope equipped with a plan-apochromat 20x,
173 0.75 NA and a 63x, 1.4 NA objective, and PMT detectors, or on a Zeiss Elyra PS1 microscope, which is
174 described below. Confocal images were acquired with optimized settings for laser power, detector
175 gains and pin hole diameters. Large (2048x2048 pixels), high-resolution images were acquired with a
176 pixel size of 0.041 µm laterally and 0.110 µm radially to facilitate the comparison with structured-

177 illumination microscopy (SIM) images. Low-resolution tile images were acquired with a pixel size of
178 0.274 µm.

179 Structured-illumination imaging was done on a Zeiss Elyra PS1 system equipped with 488, 561 and
180 642 nm, 100 mW diode lasers; fluorescence was acquired with a Zeiss plan-apochromat 63x, 1.4 NA
181 objective and an Andor iXon DU 885 EMCCD camera (1002 x 1004 pixels). Gratings were presented
182 at 5 phases and 5 rotations for every depth. Sampling interval was 110 nm axially and the
183 reconstructed super-resolution image has a pixel size of 41 nm. The fluorophore signals were
184 acquired sequentially. Reconstructions were made with built-in algorithms using ZEN 2012 SP1 black
185 (v8.1.3.484).

186 ***Electrophysiological analysis***

187 EPSPs were detected as described previously (Sierksma *et al.*, 2016) based on an EPSP minimal rate
188 of rise (>0.7 V/s) and an EPSP onset based on the third derivative. EPSPs that were present between
189 1 to 8 ms post-stimulation were categorized as 'evoked EPSPs'. Next, we grouped the evoked EPSPs
190 based on stimulus strength, latency and rate of rise. We assumed that with increasing stimulation
191 intensities previously-recruited EPSPs would still be activated. For consecutive stimulus intensities
192 Welch's *t* was calculated for the EPSP latency and the rate of rise, and both *t* values were added
193 together. When the summed *t* value was above 6 and the increase of the response rate of rise was
194 >20%, we considered the evoked EPSPs different. We visually checked whether this difference was
195 due to a new input or just a shift in activation probability of a previously-activated input. For a new
196 input its rate of rise was calculated by subtracting the rates of rise of previously identified inputs
197 when they were of similar latencies (±0.5 ms). For four recordings we found EPSPs with longer
198 latencies (Figure 1C), and for these recordings the Welch's *t* test was calculated but restricted to a
199 latency domain defined by the experimenter. For the example in Figure 1C this was 1-3 ms. Lastly,
200 the input rate of rise was checked against the spontaneously-occurring EPSP rates of rise, and the
201 defined input was only accepted if a spontaneous EPSP with a similar rate of rise also occurred.

202 In addition to the inputs identified by stimulation, we identified inputs within the spontaneous
203 EPSPs. By comparing the distribution of EPSP rates of rise of all detected EPSPs in a recording with
204 the evoked EPSPs, we could sometimes identify additional larger inputs (8 large inputs in 8 cells).
205 Within the spontaneous EPSPs, many were of a small size 0.7-2 V/s and these inputs were therefore
206 hard to identify. If small EPSPs were not evoked, we visually selected peaks from the histogram of
207 the EPSP rate of rise (Figure 1C-D) to define these smaller inputs, and added them to the dataset to
208 acknowledge their existence. However, the inputs with small EPSPs were hard to demarcate and
209 therefore likely underestimated.

210 On average, we identified 5.6 inputs per cell. For comparison, prior to synaptic elimination 5-12
211 axons connect to a principal neuron in EM studies of the mouse MNTB (Hoffpauir *et al.*, 2006). Based
212 on the comparison of spontaneous and evoked activity, in 8 out of 22 cells we were unable to
213 activate the cell's largest input. As we were able to distinguish with the stimulation a total of 80
214 synapses (both large and small) in these 22 cells, at least 1 in 10 axons (8 out of 80), but probably
215 more on the order of one in three axons (8 out of 22) were not electrically stimulated. Spontaneous
216 activity partially negated this problem, but may have introduced a bias towards the most active
217 synapses. To what extent synaptic inputs of the principal neuron are active in every spontaneous
218 activity burst is unknown, but anecdotal evidence showed extensive co-occurrence of two distinct,
219 large inputs during spontaneous bursts (Sierksma *et al.*, 2016).

220 Our method of characterizing EPSP populations in the spontaneous EPSPs has some limitations. We
221 used the presence of a clear peak in the histogram to indicate the presence of an input. However,
222 these peaks were generally distinguishable only for the larger EPSPs. Any input giving rise to an EPSP
223 smaller than 2 V/s would not be distinguishable. Nonetheless, the rates of rise of both the strongest
224 and second strongest input were very similar when estimated from either spontaneous or evoked
225 events.

226 We tested whether the strong inputs could be further subdivided based on the presence of inter-
227 event intervals that were shorter than the refractory period or the silent period within minibursts
228 (Sierksma *et al.*, 2016), but this did not lead to the identification of additional connections.
229 Altogether, we believe that our combined analysis of spontaneous and evoked responses identified
230 most synaptic inputs, except for some smaller inputs.

231 ***Image analysis***

232 Analysis of 3D-SIM image stacks was done in ImageJ using the FIJI framework (Schindelin *et al.*, 2012;
233 Schneider *et al.*, 2012). To determine the area of the postsynaptic cell body covered by the calyx of
234 Held, we segmented biocytin-stained cell bodies using a custom-designed 3D Sphere Flood fill
235 algorithm (https://github.com/ErasmusOIC/Sphere_Floodfill). The sphere had a radius of 10 pixels; a
236 voxel was included in the 3D structure when 40% of its neighboring voxels within the sphere were
237 above threshold. To account for the width of the synaptic cleft, the segmented cell body was dilated.
238 Optimal threshold and number of dilation iterations (range 4-19) were determined for each cell by
239 maximizing the covering ratio. Where needed, axonal protrusions were manually removed from the
240 segmentation. VGluT-positive structures overlapping with the dilated cell body were segmented in
241 3D using an automatic threshold (IJ_Isodata) in combination with a regular 3D Flood fill algorithm
242 (https://github.com/ErasmusOIC/FloodFill3D) using a criterion of 26 neighbors above threshold to
243 select contiguous structures. The area of the cell body was determined using the outline. The area of
244 the cell body overlapping with each contiguous VGluT-positive structure was measured. The fraction
245 of the cell body that was covered by the calyx of Held was calculated as the ratio of the covering
246 areas and the total area.

247 All images were pseudo-colored and contrasted in ImageJ. Color gamma enhancement was
248 performed with Adobe Photoshop 19.1.0. We noticed that the peak intensities of Piccolo and VGluT
249 did not overlap in SIM images. From line profiles it became clear that Piccolo labeling did overlap
250 with VGluT at lower intensities, but not at the highest VGluT intensities.

251 ***Statistical analyses***

252 Linear regression analyses against pup age were performed for the developmental effects. When the
253 developmental effect was significant, the slope of the fit is reported; when not, the average is
254 reported, and subsequently the *F*-statistic with the degrees of freedom, and the *p*-value are
255 reported. Subsequent testing on the same data was Bonferroni-corrected, and are reported as
256 'corrected *p*'. Effect sizes of a correlation are reported as Pearson's *r*. To compare prespike-
257 associated strong inputs with the other strong inputs, we performed equal-variances *t*-test for the
258 EPSP amplitude and latency. EPSP rate of rise and synaptic efficacy to trigger postsynaptic firing ($P_{AP}$)
259 were correlated with age. Age correction was performed by adding age as an explanatory variable to
260 the regression analysis. $P_{AP}$ was judged to have non-normally distributed residuals. This was
261 corrected by performing the regression analysis on the ranks. The *F*-statistic of the regression is
262 reported and the effect of prespike variable within this regression. Sigmoid and linear fits were
263 performed with Igor Pro 6.37 (WaveMetrics Inc.). To correlate the competition index with relative
264 coverage we used Spearman's rank correlation ρ. *p*-values $< 0.05$ were considered significant.

265 **Results**

266 ***Postsynaptic responses of* in vivo *stimulated fibers***

267 We made *in vivo* whole-cell recordings from principal neurons in the rat MNTB around the time the
268 calyx of Held synapse forms. A bipolar stimulation electrode was placed contralaterally from the
269 recording site to activate different axonal inputs based on their activation threshold (see Methods;
270 Figure 1A). Above a threshold of 83 ± 19 µA (mean ± SD, *n* = 30 animals, range: 65-140 µA) a field
271 potential could be evoked in the MNTB. In a total of 22 cells EPSPs could be evoked, and with
272 increasing current stimulation we typically observed either the presence of a large, all-or-none,
273 calyceal-like input, or more graded increases in EPSP size (Figure 1B). In both cases the evoked
274 responses could reach AP threshold (*n* = 16 of 22 cells). To identify the different inputs, we looked
275 for jumps in the rates of rise or changes in the latency of the evoked responses following an increase
276 in stimulus intensity, as detailed in the Methods; these discontinuities were interpreted as the
277 recruitment of a new input. A comparison of the rates of rise of the evoked EPSP with those of the
278 spontaneously-occurring EPSPs was used as a further check on the accuracy of the identified inputs
279 (Figure 1C-D). In 8 out of the 22 cells we were unable to observe the largest spontaneous EPSPs
280 following the electrical stimulation, suggesting that we did not activate the strongest input for these
281 cells. EPSP subpopulations were found with typical latencies of 1-3 and 4-8 ms (Figure 1E), as
282 described in slice studies (Banks & Smith, 1992; Hoffpauir *et al.*, 2006; Marrs & Spirou, 2012). The
283 large EPSPs always belonged to the subpopulation with 1-3 ms delays (Figure 1E). On average the
284 EPSP latencies became smaller during the first postnatal week (Figure 1F). In addition to early
285 myelination (Rozeik & Von Keyserlingk, 1987; Hamano *et al.*, 1996), an increase in axon diameter
286 and/or conductances may have contributed to this decrease in latency. The different subpopulations
287 may reflect different developmental stages among the calycigenic axons.

288 Within this developmental period the principal neuron passes through a stage of exuberant synaptic
289 connectivity (Holcomb *et al.*, 2013). In addition to the 22 cells in which we recorded both evoked

290 and spontaneous EPSPs, we recorded in 10 cells only the spontaneous activity. In total, we identified
291 180 putative inputs in 32 cells, 5.6 ± 0.3 per cell (mean ± SEM). The distribution of input rate of rise
292 was skewed to the right (Figure 2A). By sorting per cell the inputs on their mean EPSP rate of rise, a
293 discontinuity was observed at about 10 V/s (Figure 2A-B), which we used as a threshold to
294 distinguish between weak and strong EPSPs. To have a measure of synaptic competition, we
295 calculated the competition index, which is defined as the ratio of the rates of rise of the second
296 strongest and the strongest input (Figure 2C). The competition index decreased during development
297 (-0.07 ± 0.02 $day^{-1}$, $F_{1,30} = 11$, $p = 0.002$). This decrease can signify both an increase of the strongest
298 input rate of rise and a reduction of the second strongest input. We therefore plotted the two
299 against each other (Figure 2D). The rate of rise of the strongest input clearly increased during
300 development (4.2 ± 1.1 V $s^{-1}$ $day^{-1}$, $F_{1,30} = 14$, corrected $p = 0.001$), while the rate of rise of the second
301 strongest did not change (3.7 ± 0.2 V/s, $F_{1,30} = 2.1$, corrected $p = 0.3$). Inputs identified using
302 stimulation or spontaneous activity had similar rates of rise for both the strongest (stim.: 19 ± 3 V/s,
303 n = 14; spont.: 16 ± 2 V/s, n = 18) and the second strongest input (stim.: 3.9 ± 0.3 V/s, n = 13; spont.:
304 3.6 ± 0.3 V/s, n = 19), suggesting that the selective developmental increase in the rate of rise of the
305 largest inputs was unrelated to the identification method. In contrast to what may have been
306 expected for competing inputs, the developmental increase in strength of the strongest input did
307 not coincide with a decrease in the second strongest input.

308 ***Strong inputs and prespikes***

309 The effects of electrical stimulation of the calyx of Held synapse have been extensively studied in
310 slices (Borst & Soria van Hoeve, 2012), but equivalent *in vivo* recordings have not yet been reported.
311 In nine cells we could activate an input associated with an EPSP >10 V/s that could easily be
312 distinguished from the other EPSPs. These inputs could be activated with a threshold current of 0.24
313 ± 0.05 mA (mean ± SEM; range 0.12 – 0.40 mA), although the reliability of activation with current
314 above threshold varied between pups (83 ± 7% of the stimulations, mean ± SEM; range 59-100%).
315 The average latency of the input's EPSP was 2.1 ± 0.1 ms (mean ± SEM, range 1.6 – 2.5 ms) with little

316 jitter between trials (SD/mean: 2.3 ± 0.4%, range 1.0-3.8%). Given the distance of 500-1000 µm
317 between the stimulation and recording electrode and a synaptic delay of ~0.5 ms, the propagation
318 speed can be estimated to be in the order of 1 m/s. The AP travel time became less variable with
319 development (jitter vs. age, $r$ = -0.75, -0.7 ± 0.2% per day, $F_{1,7}$ = 9.0, $p$ = 0.02). In addition, a decrease
320 in latency ($r$ = -0.7, -0.18 ± 0.07 ms/day, $F_{1,7}$ = 5.6, $p$ = 0.05) suggested a developmental increase in
321 conduction speed. This increase is likely underestimated, as we positioned the stimulation electrode
322 as contralaterally as was permitted by the cranial window to be able to separate the stimulus
323 artefact from the responses. These developmental changes will contribute towards the precise
324 timing of the calyx of Held in adult, hearing animals.

325 The calyx of Held can typically be identified in postsynaptic recordings by the presence of a prespike,
326 a small deflection preceding the large EPSPs (Forsythe, 1994; Borst *et al.*, 1995; Lorteije *et al.*, 2009).
327 Prespikes can already be detected in the first postnatal week (Crins *et al.*, 2011; Sierksma *et al.*,
328 2016). We therefore inspected every strong input whether a prespike was present (Figure 3A). In
329 four of four cells >P5, six of ten cells of P4-5, and in none of six P2-3 cells large EPSPs were preceded
330 by a prespike (Figure 3B). Hence, the presence of the prespike before a large EPSP was more likely at
331 older ages ($r$ = 0.7); a fit with a logistic function yielded a mid-point of 4.1 ± 0.4 days postnatally
332 (mean ± SD) and a steepness of 0.7 ± 0.4 days, suggesting that within two days most strong inputs
333 will become associated with a prespike. This switch may be explained by an increase in the currents
334 over the calyceal membrane facing the synaptic cleft or by an increase in the coupling between the
335 pre- and the postsynaptic membranes. The currents depend on apposition area (Hoffpauir *et al.*,
336 2006; Holcomb *et al.*, 2013), time course of the calyceal AP, which accelerates considerably during
337 early development (Taschenberger & von Gersdorff, 2000; Sierksma & Borst, 2017), isochronicity of
338 the presynaptic currents, and the subcellular distribution of presynaptic ion channels. In addition,
339 the coupling depends on synaptic cleft resistivity and postsynaptic admittance (Savtchenko, 2007).
340 The rapid change in most of these properties during this period should underlie the emergence of
341 the prespike.

342 As we observed strong inputs with and without prespike, we asked whether their properties were
343 different. For the inputs that were electrically stimulated, the strong inputs with and without a
344 prespike had a latency of 2.1 ± 0.2 ms and 2.2 ± 0.1 ms, respectively (Figure 3C, n = 4 and 5 inputs, $t_7$
345 = 0.5, $r$ = -0.2, $p$ = 0.6). For the EPSP rate of rise, amplitude and the efficacy to trigger a postsynaptic
346 AP ($P_{AP}$), we included the strong inputs that were identified in the spontaneous activity. The EPSP
347 rate of rise was 28 ± 2 V/s versus 19 ± 2 V/s (Figure 3D, age correction, $F_{2,17}$ = 5.3, effect of prespike,
348 5 ± 4 V/s, $t_{17}$ = 1.2, $p$ = 0.3) and had a coefficient of variation in the range of 7-38%. EPSP amplitude,
349 which did not significantly correlate with age ($r$ = 0.2), was 19.6 ± 1.1 mV versus 15.6 ± 1.5 mV ($t_{18}$ =
350 2.1, $r$ = 0.45, $p$ = 0.05). As these EPSPs typically triggered an AP (75 ± 7%, mean ± SEM; range 11-
351 100%), their amplitudes are underestimated. The fraction of EPSPs that triggered a postsynaptic AP
352 was 0.88 ± 0.07 versus 0.63 ± 0.11 (Figure 3E, rank-transform and age correction, $F_{2,17}$ = 5.4, effect of
353 prespike: 7 ± 3, $t_{17}$ = 2.6, $p$ = 0.02). Overall, prespike-associated inputs triggered postsynaptic activity
354 more effectively. Still, some terminals that did not generate a detectable prespike were comparable
355 to the calyces in strength and efficacy, as we observed before (Sierksma *et al.*, 2016). Next, we will
356 discuss the relation between physiological properties and the underlying synaptic structure.

357 ***The active zone protein Piccolo in the neonatal auditory brainstem***

358 The dramatic developmental change in the glutamatergic innervation of MNTB neurons can be
359 visualized by VGluT immunolabeling (Rodríguez-Contreras *et al.*, 2008). One limitation is that VGluT
360 labeling does not mark release sites, which can complicate the identification of the target neuron.
361 We therefore tested whether Piccolo, an active zone protein known to be already present in P9
362 calyces (Dondzillo *et al.*, 2010), could be used to visualize the release face of terminals within this
363 developmental period. Already at P3-4, Piccolo-labeling was found throughout the superior olivary
364 complex (SOC) in all auditory nuclei ($n$ = 8 rats; Figure 4A). Although the staining was not particularly
365 strong in the MNTB, it clearly co-labeled large perisomatic structures containing VGluT (Figure 4B).
366 As early as P2, the Piccolo labeling could delineate an edge of the larger VGluT-clusters (Figure 4C, $n$
367 = 2 of 5 P2 animals). Piccolo puncta were also found outside the somatic regions of the MNTB, and a

368 Piccolo punctum was occasionally found within the soma of a principal cell (Figure 4C). Generally,
369 when imaged with confocal microscopy, the Piccolo edges appeared to be composed of individual
370 spots, which were close to the diffraction limit (Figure 4C-D). We turned to structured-illumination
371 microscopy (Gustafsson, 2005), which revealed that the Piccolo clusters were indeed composed of
372 multiple spots (Figure 4D). These spots were also found in biocytin-filled calyces, indicating that
373 Piccolo can be present in the active zones of the calyx of Held at P5 (*n* = 11 of 12 calyces; Figure 4E).
374 Piccolo thus identifies the release face of synapses and thereby can help to identify the target of the
375 VGluT cluster in the case of axosomatic terminals (Figure 4C-D). However, dendritic synapses cannot
376 be reliably identified without labeling the postsynaptic neuron.

377 ***Structure-function correlation within and across cells***

378 From the 32 recorded cells, we recovered 20 cells with immunolabeling for VGluT (1 P2, 7 P3, 8 P4, 2
379 P5, 1 P6, 1 P7). For these cells we segmented the soma and the VGluT clusters surrounding the soma
380 using a new, semi-automatic procedure (see Methods, Figure 5A). This segmentation takes into
381 account that a VGluT cluster may have multiple contact points with the soma by clustering
382 connected voxels. A VGluT cluster is thus defined as a contiguous structure of VGluT-positive voxels
383 and VGluT clusters, by definition, were not in contact with each other. The total somatic surface was
384 620 ± 60 $\mu m^2$ (mean ± SEM, n = 20), which is comparable to earlier estimates (Sommer *et al.*, 1993;
385 Hoffpauir *et al.*, 2006). We observed that multiple VGluT clusters contacted the postsynaptic cell, of
386 which most had a postsynaptic contact area <3 $\mu m^2$ (Figure 5B-C). The total postsynaptic area that
387 was covered by VGluT ranged from 2.4 $\mu m^2$ to 76.5 $\mu m^2$. As calyces can cover >50% of the soma
388 (Sätzler *et al.*, 2002; Hoffpauir *et al.*, 2006), our segmentation of VGluT may give us only a lower-
389 bound approximation of its size. The difference may reflect a delay in VGluT filling after calyx
390 formation (Rodríguez-Contreras *et al.*, 2008). For each cell we identified the largest and second
391 largest VGluT cluster. The contact area of the largest cluster on the postsynaptic cell ranged from 0.4
392 $\mu m^2$ to 59.7 $\mu m^2$ (mean 13.9 ± 3.5 $\mu m^2$). For the second largest cluster it ranged from 0.3 $\mu m^2$ to 10.0
393 $\mu m^2$ (2.5 ± 0.7 $\mu m^2$). For 3 cells the Piccolo labeling failed. For 9 cells we could see clear Piccolo

394 labeling coinciding with the largest VGluT cluster directed towards the biocytin-filled cell. For 8 cells
395 VGluT clusters surrounding the biocytin-labeled soma did not show clear Piccolo labeling, but Piccolo
396 coincided with VGluT in the surrounding tissue. More in-depth analysis of the Piccolo clusters was
397 not attempted because of reconstruction-related noise.

398 If the size of the VGluT cluster is a useful estimate of the size of the terminal, then it should predict
399 the presence and amplitude of a prespike in our *in vivo* recordings. In five of the recovered cells we
400 recorded a prespike. The size of the VGluT cluster was moderately correlated with the presence of a
401 prespike ($\rho = 0.63$, Figure 5G). The largest VGluT cluster was 30.0 ± 7.5 $\mu m^2$ in the cells in which we
402 recorded a prespike. This was significantly larger than in the cells without a prespike (8.5 ± 2.9 $\mu m^2$,
403 $t_{18} = 3.3$, $p = 0.004$). Next, we compared the prespike peak-to-peak amplitude with the size of the
404 largest VGluT cluster. We excluded one of the recordings, in which the prespikes had an amplitude
405 of 15 mV. In this recording a small patch of calyceal membrane may have been present within the
406 electrode tip (Forsythe, 1994). As the calyx was not stained for biocytin, the membrane of the calyx
407 was apparently not damaged by the pipette. For the remaining prespikes the average amplitudes
408 were 0.11, 0.26, 0.30 and 0.37 mV, which corresponded with values of 19.2, 23.1, 25.6 and 59.7 $\mu m^2$
409 for the largest VGluT cluster (r = 0.8). We cannot exclude that this strong correlation was by chance
410 ($F_{1,2} = 3$, $p = 0.2$). Also, we observed VGluT clusters with similar contact area among the cells from
411 which we did not record a prespike. Altogether, the size of the largest VGluT cluster may indicate the
412 presence of a large terminal, but it is unlikely to reveal the entire contact area made by the terminal.

413 As synaptic strength depends more on glutamate release than on terminal size, the observed VGluT
414 cluster may still be a good approximation of synaptic strength. We therefore compared synaptic
415 strength with the contact area of VGluT clusters (Figure 5E). The size of the strongest input was
416 correlated to the size of the largest VGluT cluster (log-transform, $r = 0.8$, $F_{1,18} = 26$, $p < 0.001$). The
417 structure-strength relation could be approximated by EPSP (V/s) = $\beta$ area$^{\alpha}$ with $\beta = 6.8 \pm 0.9$ V $s^{-1}$ $\mu m^{-2\alpha}$
418 and $\alpha = 0.35 \pm 0.06$. Thus, the input strength was correlated with the cube root of VGluT area. For

419 the older pups (2 P5, 1 P6 and 1 P7 cell) the structure-function relation was underestimated; three of
420 four synapses were stronger than expected from their apposition area. This may indicate that there
421 is a developmental change in the structure-function relation or that the total vesicle-loaded contact
422 of giant synapses is underestimated as the largest VGluT cluster may be only a small part of the
423 synapse.

424 Calyces that innervate a multi-calyceal principal cell are filled with synaptic vesicles (Holcomb *et al.*,
425 2013). The size of the second largest VGluT cluster was not correlated with the size of the second
426 strongest input ($r$ = -0.1, $F_{1,16}$ = 0.3, $p$ = 0.6). However, we cannot be sure whether multiple VGluT
427 clusters are independent inputs or belong to the same synapse. We therefore compared the
428 competition index to the ratio of the largest VGluT cluster to the total somatic surface contacted by
429 VGluT. This ratio ranged from 9-98% (on average 42 ± 7%) and was negatively correlated to the
430 competition index (Figure 5F, $F_{2,17}$ = 13, $p$ < 0.001, age correction, ρ = -0.7). We thus conclude that
431 we did not find evidence for large discrepancies between the physiological and morphological size of
432 inputs at the developing calyx of Held synapse. A large VGluT cluster likely indicates the presence of
433 a strong input that is much stronger than the other inputs of its target neuron.

434 In the case of multi-calyceal innervation, the different calyces each occupy a contiguous area,
435 sometimes at opposite sides of the target neuron (Holcomb *et al.*, 2013). This type of multi-
436 innervation was not observed here (Figure 5B, C and F).

437 **Discussion**

438 In this study we combined *in vivo* electrophysiology with immunolabeling of the developing calyx of
439 Held synapse. With afferent stimulation we identified multiple inputs for each principal neuron.
440 Increasing stimulation levels showed either a graded increase or a sudden, large jump in the rate of
441 rise of the response. The strongest inputs across cells showed a shorter latency. The strongest inputs
442 were typically at least twice as strong as the other inputs. This divergence increased during
443 development with little change in the strength of the second strongest input. We found that in the
444 first postnatal week Piccolo is already present within perisomatic VGluT clusters, which are putative
445 calyceal terminals. The contact surface of the largest VGluT cluster correlated with the strength of
446 the strongest input *in vivo*. Furthermore, the relative coverage of the largest VGluT cluster
447 correlated with the relative strength of the strongest to the second strongest input. Overall, synaptic
448 structure thus correlated with synaptic strength *in vivo*. The association of a strong input with a
449 prespike became more likely during development. Prespike-associated inputs were more effective in
450 triggering postsynaptic activity, but some inputs without a prespike had similar properties.

451 ***Calyceal competition during development?***

452 The prevalence of multiple calyces on a single principal MNTB neuron is a subject of debate. In slice
453 recordings multiple strong inputs have been observed (Bergsman *et al.*, 2004; Hoffpauir *et al.*, 2006;
454 Hoffpauir *et al.*, 2010), and structural evidence for the presence of multiple large terminals on
455 rodent MNTB neurons has also been obtained (Wimmer *et al.*, 2004; Hoffpauir *et al.*, 2006; Holcomb
456 *et al.*, 2013; Matho, 2013). Although only a minority (up to 10%) of neurons is persistently
457 innervated by multiple calyces (Holcomb *et al.*, 2013; Matho, 2013), as many as half of the principal
458 neurons are putatively contacted during development by multiple large terminals (Holcomb *et al.*,
459 2013). On the other hand, to our knowledge, not a single conclusive example of multi-calyceal
460 innervation has been reported for *in vivo* studies of the adult MNTB. In this developmental study,
461 neither our *in vivo* recordings nor our synapse reconstructions revealed multi-calyceal innervation,
462 but weak calyces with a low density of VGluT, or inputs that are unable to generate prespikes would

463 not have been identified as such. In our earlier study, three out of 132 cells were found that each
464 had two strong inputs that could be separated based on the presence or absence of a prespike
465 (Sierksma *et al.*, 2016). As we observed large VGluT clusters without the identification of prespike-
466 associated input for their target cells, these cases may have been examples of multi-calyceal
467 innervation, but we cannot exclude that one of the inputs was dendritic. From our earlier (3/132
468 cells) and the current (0/32 cells) experiments, we thus estimate that <10% of rat principal neurons
469 has multi-calyceal innervation during development.

470 Initial neural connectivity is extensively remodeled to form the final neural circuitry (Katz & Shatz,
471 1996). As the remodeling will strengthen proper inputs and eliminate improper ones, it is viewed as
472 a competition between inputs with their activity and efficacy in triggering postsynaptic APs as
473 instructive cues. The principal neuron has an extreme developmental outcome by allowing the
474 formation of only one giant synapse amidst multiple calycigenic inputs (Morest, 1968; Baydyuk *et al.*,
475 2016). The presence of competition has been evaluated by the (relative) contact surface (Holcomb *et*
476 *al.*, 2013) or by the (relative) strength of the inputs (Hoffpauir *et al.*, 2010; Sierksma *et al.*, 2016).
477 Here, we compared a structural and a functional measure for competition, and generally observed a
478 good match between the two. One limitation is that our immunolabeling did not allow the
479 unambiguous identification of different inputs based on the VGluT clusters, which limits us to give a
480 definite measure of structural competition. Still, the observed match between VGluT relative
481 coverage and the competition index indicates that the physiological and morphological development
482 are linked.

483 Two types of competition have been contrasted previously (Holcomb *et al.*, 2013), exemplified by
484 the neuromuscular junction (NMJ) and the cerebellar climbing fiber-Purkinje cell synapse (CF-PC).
485 Before mono-innervation is established in the case of the NMJ, one input becomes >4 fold stronger
486 than the other ones by both an increase of the strongest and a decrease of the other inputs (Colman
487 *et al.*, 1997). As NMJ inputs compete at and for a small patch of the muscle membrane (Sanes &

488 Lichtman, 1999; Darabid *et al.*, 2014), the expansion of one NMJ necessarily involves the shrinkage
489 of another, as reflected in the opposing changes in strength. In contrast, CFs compete at the soma
490 for the apical dendrite (Watanabe & Kano, 2011). A fourfold strengthening of the strongest input
491 was observed (Hashimoto & Kano, 2003) while other inputs remained constant (Bosman *et al.*,
492 2008). Subsequently, one of the immature CFs is allowed to translocate to the apical dendrite
493 (Hashimoto *et al.*, 2009; Watanabe & Kano, 2011), ending the competition (Carrillo *et al.*, 2013). We
494 observed that the strongest input increases in strength without a substantial change for the second
495 strongest. This may indicate that they do not compete for overlapping synaptic domains (Holcomb *et*
496 *al.*, 2013). In addition, we observed that the strongest input can already be four times stronger than
497 the second strongest while its coverage is still low. This might indicate that the increase in strength
498 precedes and instructs the expansion (Hoffpauir *et al.*, 2010). The inverse, a large VGluT cluster with
499 a high competition index, was not observed, suggesting that VGluT filling of an axosomatic terminal
500 might be a late stage in maturation (Rodríguez-Contreras *et al.*, 2008).

501 ***Structure-function relation for the developing calyx of Held synapse***

502 The presence of a prespike indicates the innervation by a giant terminal (Forsythe, 1994). In this
503 study four cells with a prespike-associated input had a large VGluT cluster and one cell did not. This
504 may indicate that the terminal was larger than revealed by VGluT labeling (Rodríguez-Contreras *et*
505 *al.*, 2008). Four cells were observed where a large VGluT cluster did not match with a prespike-
506 associated input. By recording in each pup only a single neuron, we ensured that the retrieved cell
507 was the recorded cell, as evidenced by the clear match between synapse strength and VGluT cluster.
508 The capacitive filtering by the soma may have obscured small prespikes that might have been
509 detectable in voltage-clamp recordings. There are also a number of biological factors that influence
510 the prespike amplitude (see Results). For now, the low number of cells with a discrepancy between
511 structure and morphology does not warrant any firm conclusions. Experimental observations on the
512 relation between presynaptic AP and the prespike have so far been qualitative (Forsythe, 1994; Borst
513 *et al.*, 1995; Wang *et al.*, 2017). Experimental and computational studies on the prespike

514 (Savtchenko, 2007) based on exact morphology (Spirou *et al.*, 2008) may give us an answer under
515 which conditions a calyx generates a prespike.

516 From our structure-function analyses we found that VGluT labeling closely follows the strength of
517 the strongest input. This VGluT cluster likely represents the total pool of glutamatergic vesicles in the
518 calyx of Held (Rodríguez-Contreras *et al.*, 2008). The relation between the size of this pool and
519 synaptic strength is complex, depending on among others quantal size, release probability, and
520 number of release sites (Atwood & Karunanithi, 2002; Schneggenburger & Forsythe, 2006; Borst &
521 Soria van Hoeve, 2012). We found a cube root relation between VGluT contact surface and EPSP rate
522 of rise, suggesting that the increase in vesicle pool is relatively ineffective in increasing synaptic
523 strength. This can be partially explained by homeostatic plasticity of postsynaptic excitability
524 (Hoffpauir *et al.*, 2010; Rusu & Borst, 2011; Sierksma *et al.*, 2016). Another possibility is that the
525 input also has formed dendritic synapses (Rodríguez-Contreras *et al.*, 2008; Holcomb *et al.*, 2013).
526 However, the EPSC-EPSP relation saturates for large EPSCs (Lorteije *et al.*, 2009; Sierksma *et al.*,
527 2016), indicating that for weak inputs (small clusters) the relation may be more linear.

528 For the study of the relationship between structure and function, the calyx of Held synapse has the
529 advantage of an axosomatic, (putative) one-to-one innervation facilitating the identification of the
530 strongest input *in vivo* with the largest cluster *ex vivo*. An even more direct relationship might be
531 possible following simultaneous electrophysiology and calcium imaging *in vivo* (Winnubst *et al.*,
532 2015). Subsequent reconstruction of the synapses after *in vivo* imaging (Liang *et al.*, 2018) would
533 allow a structure-function description for multiple synapses of a single cell. Such studies may further
534 define the relationship between morphological and functional properties of the precursors of the
535 calyx of Held. Finally, longitudinal imaging might reveal some of the dynamics associated with the
536 formation of the calyx of Held (Rodríguez-Contreras *et al.*, 2008).

537 **References**


538 Atwood HL & Karunanithi S. (2002). Diversification of synaptic strength: presynaptic elements. *Nat*
539 *Rev Neurosci* **3,** 497-516.

540 Banks MI & Smith PH. (1992). Intracellular recordings from neurobiotin-labeled cells in brain slices of
541 the rat medial nucleus of the trapezoid body. *Journal of Neuroscience* **12,** 2819-2837.

542 Baydyuk M, Xu J & Wu LG. (2016). The calyx of Held in the auditory system: Structure, function, and
543 development. *Hear Res* **338,** 22-31.

544 Bergsman JB, De Camilli P & McCormick DA. (2004). Multiple large inputs to principal cells in the
545 mouse medial nucleus of the trapezoid body. *J Neurophysiol* **92,** 545-552.

546 Borst JGG, Helmchen F & Sakmann B. (1995). Pre- and postsynaptic whole-cell recordings in the
547 medial nucleus of the trapezoid body of the rat. *J Physiol* **489,** 825-840.

548 Borst JGG & Soria van Hoeve J. (2012). The calyx of Held synapse: from model synapse to auditory
549 relay. *Annual Review of Physiology* **74,** 199-224.

550 Bosman LWJ, Takechi H, Hartmann J, Eilers J & Konnerth A. (2008). Homosynaptic long-term synaptic
551 potentiation of the "winner" climbing fiber synapse in developing Purkinje cells. *J Neurosci*
552 **28,** 798-807.

553 Carrillo J, Nishiyama N & Nishiyama H. (2013). Dendritic translocation establishes the winner in
554 cerebellar climbing fiber synapse elimination. *J Neurosci* **33,** 7641-7653.

555 Chuhma N & Ohmori H. (1998). Postnatal development of phase-locked high-fidelity synaptic
556 transmission in the medial nucleus of the trapezoid body of the rat. *J Neurosci* **18,** 512-520.

557 Colman H, Nabekura J & Lichtman JW. (1997). Alterations in synaptic strength preceding axon
558 withdrawal. *Science* **275,** 356-361.

559 Crins TTH, Rusu SI, Rodríguez-Contreras A & Borst JGG. (2011). Developmental changes in short-term
560 plasticity at the rat calyx of Held synapse. *J Neurosci* **31,** 11706-11717.

561 Darabid H, Perez-Gonzalez AP & Robitaille R. (2014). Neuromuscular synaptogenesis: coordinating
562 partners with multiple functions. *Nature Reviews Neuroscience* **15,** 703.

563 Denk W & Horstmann H. (2004). Serial block-face scanning electron microscopy to reconstruct three-
564 dimensional tissue nanostructure. *PLOS Biology* **2,** e329.
565 Dondzillo A, Sätzler K, Horstmann H, Altrock WD, Gundelfinger ED & Kuner T. (2010). Targeted three-
566 dimensional immunohistochemistry reveals localization of presynaptic proteins Bassoon and
567 Piccolo in the rat calyx of Held before and after the onset of hearing. *J Comp Neurol* **518,**
568 1008-1029.
569 Forsythe ID. (1994). Direct patch recording from identified presynaptic terminals mediating
570 glutamatergic EPSCs in the rat CNS, *in vitro*. *J Physiol* **479,** 381-387.
571 Gundelfinger ED, Reissner C & Garner CC. (2016). Role of Bassoon and Piccolo in assembly and
572 molecular organization of the active zone. *Frontiers in Synaptic Neuroscience* **7**.
573 Gustafsson MGL. (2005). Nonlinear structured-illumination microscopy: Wide-field fluorescence
574 imaging with theoretically unlimited resolution. *Proceedings of the National Academy of*
575 *Sciences of the United States of America* **102,** 13081-13086.
576 Hamano K, Iwasaki N, Takeya T & Takita H. (1996). A quantitative analysis of rat central nervous
577 system myelination using the immunohistochemical method for MBP. *Dev Brain Res* **93,** 18-
578 22.
579 Hashimoto K, Ichikawa R, Kitamura K, Watanabe M & Kano M. (2009). Translocation of a "winner"
580 climbing fiber to the Purkinje cell dendrite and subsequent elimination of "losers" from the
581 soma in developing cerebellum. *Neuron* **63,** 106-118.
582 Hashimoto K & Kano M. (2003). Functional differentiation of multiple climbing fiber inputs during
583 synapse elimination in the developing cerebellum. *Neuron* **38,** 785-796.
584 Held H. (1893). Die centrale Gehörleitung. *Archiv fur Anatomie und Physiologie, Anatomie Abtheil***,**
585 201-248.
586 Hoffpauir BK, Grimes JL, Mathers PH & Spirou GA. (2006). Synaptogenesis of the calyx of Held: rapid
587 onset of function and one-to-one morphological innervation. *J Neurosci* **26,** 5511-5523.

588 Hoffpauir BK, Kolson DR, Mathers PH & Spirou GA. (2010). Maturation of synaptic partners:
589 functional phenotype and synaptic organization tuned in synchrony. *J Physiol* **588,** 4365-
590 4385.
591 Holcomb PS, Hoffpauir BK, Hoyson MC, Jackson DR, Deerinck TJ, Marrs GS, Dehoff M, Wu J, Ellisman
592 MH & Spirou GA. (2013). Synaptic inputs compete during rapid formation of the calyx of
593 Held: a new model system for neural development. *J Neurosci* **33,** 12954-12969.
594 Kandler K & Friauf E. (1993). Pre- and postnatal development of efferent connections of the cochlear
595 nucleus in the rat. *Journal of Comparative Neurology* **328,** 161-184.
596 Katz LC & Shatz CJ. (1996). Synaptic activity and the construction of cortical circuits. *Science* **274,**
597 1133-1138.
598 Kuwabara N, DiCaprio RA & Zook JM. (1991). Afferents to the medial nucleus of the trapezoid body
599 and their collateral projections. *Journal of Comparative Neurology* **314,** 684-706.
600 Liang L, Fratzl A, Goldey G, Ramesh RN, Sugden AU, Morgan JL, Chen C & Andermann ML. (2018). A
601 fine-scale functional logic to convergence from retina to thalamus. *Cell* **173,** 1343-1355
602 e1324.
603 Lorteije JAM, Rusu SI, Kushmerick C & Borst JGG. (2009). Reliability and precision of the mouse calyx
604 of Held synapse. *J Neurosci* **29,** 13770-13784.
605 Marrs GS & Spirou GA. (2012). Embryonic assembly of auditory circuits: spiral ganglion and
606 brainstem. *J Physiol* **590,** 2391-2408.
607 Matho KSH. (2013). Structure and dynamism in a central neural circuit in adulthood and postnatal
608 development. In *École Doctorale Cerveau, Cognition, Comportement*. Université Pierre et
609 Marie Curie, Paris, France.
610 Morest DK. (1968). The growth of synaptic endings in the mammalian brain: a study of the calyces of
611 the trapezoid body. *Zeitschrift für Anatomie und Entwicklungsgeschichte* **127,** 201-220.
612 Qiu X, Zhu Q & Sun J. (2015). Quantitative analysis of vesicle recycling at the calyx of Held synapse.
613 *Proceedings of the National Academy of Sciences* **112,** 4779-4784.

614 Rodríguez-Contreras A, de Lange RPJ, Lucassen PJ & Borst JGG. (2006). Branching of calyceal
615 afferents during postnatal development in the rat auditory brainstem. *J Comp Neurol* **496,**
616 214-228.
617 Rodríguez-Contreras A, van Hoeve JS, Habets RLP, Locher H & Borst JGG. (2008). Dynamic
618 development of the calyx of Held synapse. *Proc Natl Acad Sci U S A* **105,** 5603-5608.
619 Rollenhagen A & Lübke JHR. (2006). The morphology of excitatory central synapses: from structure
620 to function. *Cell Tissue Res* **326,** 221-237.
621 Rozeik C & Von Keyserlingk D. (1987). The sequence of myelination in the brainstem of the rat
622 monitored by myelin basic protein immunohistochemistry. *Developmental Brain Research*
623 **35,** 183-190.
624 Rusu SI & Borst JGG. (2011). Developmental changes in intrinsic excitability of principal neurons in
625 the rat medial nucleus of the trapezoid body. *Dev Neurobiol* **71,** 284-295.
626 Sanes JR & Lichtman JW. (1999). Development of the vertebrate neuromuscular junction. *Annu Rev*
627 *Neurosci* **22,** 389-442.
628 Sätzler K, Söhl LF, Bollmann JH, Borst JGG, Frotscher M, Sakmann B & Lübke JHR. (2002). Three-
629 dimensional reconstruction of a calyx of Held and its postsynaptic principal neuron in the
630 medial nucleus of the trapezoid body. *J Neurosci* **22,** 10567-10579.
631 Savtchenko LP. (2007). Bilateral processing in chemical synapses with electrical 'ephaptic' feedback:
632 a theoretical model. *Math Biosci* **207,** 113-137.
633 Schindelin J, Arganda-Carreras I, Frise E, Kaynig V, Longair M, Pietzsch T, Preibisch S, Rueden C,
634 Saalfeld S, Schmid B, Tinevez JY, White DJ, Hartenstein V, Eliceiri K, Tomancak P & Cardona
635 A. (2012). Fiji: an open-source platform for biological-image analysis. *Nat Methods* **9,** 676-
636 682.
637 Schneggenburger R & Forsythe ID. (2006). The calyx of Held. *Cell Tissue Res* **326,** 311-337.
638 Schneider CA, Rasband WS & Eliceiri KW. (2012). NIH Image to ImageJ: 25 years of image analysis.
639 *Nat Methods* **9,** 671-675.

640 Sierksma MC & Borst JGG. (2017). Resistance to action potential depression of a rat axon terminal in
641 vivo. *Proceedings of the National Academy of Sciences* **114,** 4249-4254.
642 Sierksma MC, Tedja MS & Borst JGG. (2016). *In vivo* matching of postsynaptic excitability with
643 spontaneous synaptic inputs during formation of the rat calyx of Held synapse. *J Physiol* **595,**
644 207-231.
645 Sommer I, Lingenhöhl K & Friauf E. (1993). Principal cells of the rat medial nucleus of the trapezoid
646 body: an intracellular in vivo study of their physiology and morphology. *Experimental Brain*
647 *Research* **95,** 223-239.
648 Soria Van Hoeve J & Borst JGG. (2010). Delayed appearance of the scaffolding proteins PSD-95 and
649 Homer-1 at the developing rat calyx of Held synapse. *J Comp Neurol* **518,** 4581-4590.
650 Spirou GA, Chirila FV, von Gersdorff H & Manis PB. (2008). Heterogeneous $Ca^{2+}$ influx along the adult
651 calyx of Held: a structural and computational study. *Neuroscience* **154,** 171-185.
652 Südhof Thomas C. (2012). The presynaptic active zone. *Neuron* **75,** 11-25.
653 Taschenberger H, Leão RM, Rowland KC, Spirou GA & von Gersdorff H. (2002). Optimizing synaptic
654 architecture and efficiency for high-frequency transmission. *Neuron* **36,** 1127-1143.
655 Taschenberger H & von Gersdorff H. (2000). Fine-tuning an auditory synapse for speed and fidelity:
656 developmental changes in presynaptic waveform, EPSC kinetics, and synaptic plasticity. *J*
657 *Neurosci* **20,** 9162-9173.
658 Wang T, van Woerden GM, Elgersma Y & Borst JGG. (2017). Enhanced transmission at the calyx of
659 Held synapse in a mouse model for Angelman syndrome. *Front Cell Neurosci* **11,** 418.
660 Watanabe M & Kano M. (2011). Climbing fiber synapse elimination in cerebellar Purkinje cells. *Eur J*
661 *Neurosci* **34,** 1697-1710.
662 Wimmer VC, Nevian T & Kuner T. (2004). Targeted in vivo expression of proteins in the calyx of Held.
663 *Pflügers Arch* **449,** 319-333.
664 Winnubst J, Cheyne JE, Niculescu D & Lohmann C. (2015). Spontaneous activity drives local synaptic
665 plasticity in vivo. *Neuron* **87,** 399-410.

666 Xiao L, Michalski N, Kronander E, Gjoni E, Genoud C, Knott G & Schneggenburger R. (2013). BMP
667 signaling specifies the development of a large and fast CNS synapse. *Nat Neurosci* **16,** 856-
668 864.
669 Yu WM & Goodrich LV. (2014). Morphological and physiological development of auditory synapses.
670 *Hear Res* **311,** 3-16.

671

672

673 ***Figure list***

674 **Figure 1. Responses to current stimulation of developing calycigenic axons.**

675 **Figure 2. Synaptic competition in MNTB follows the expansion of the strongest input without**

676 **changing the second strongest input.**

677 **Figure 3. Comparison of strong inputs with and without prespikes.**

678 **Figure 4. Developmental expression of Piccolo in the MNTB.**

679 **Figure 5. Contact area of perisomatic VGluT clusters correlates with synaptic strength *in vivo***

680

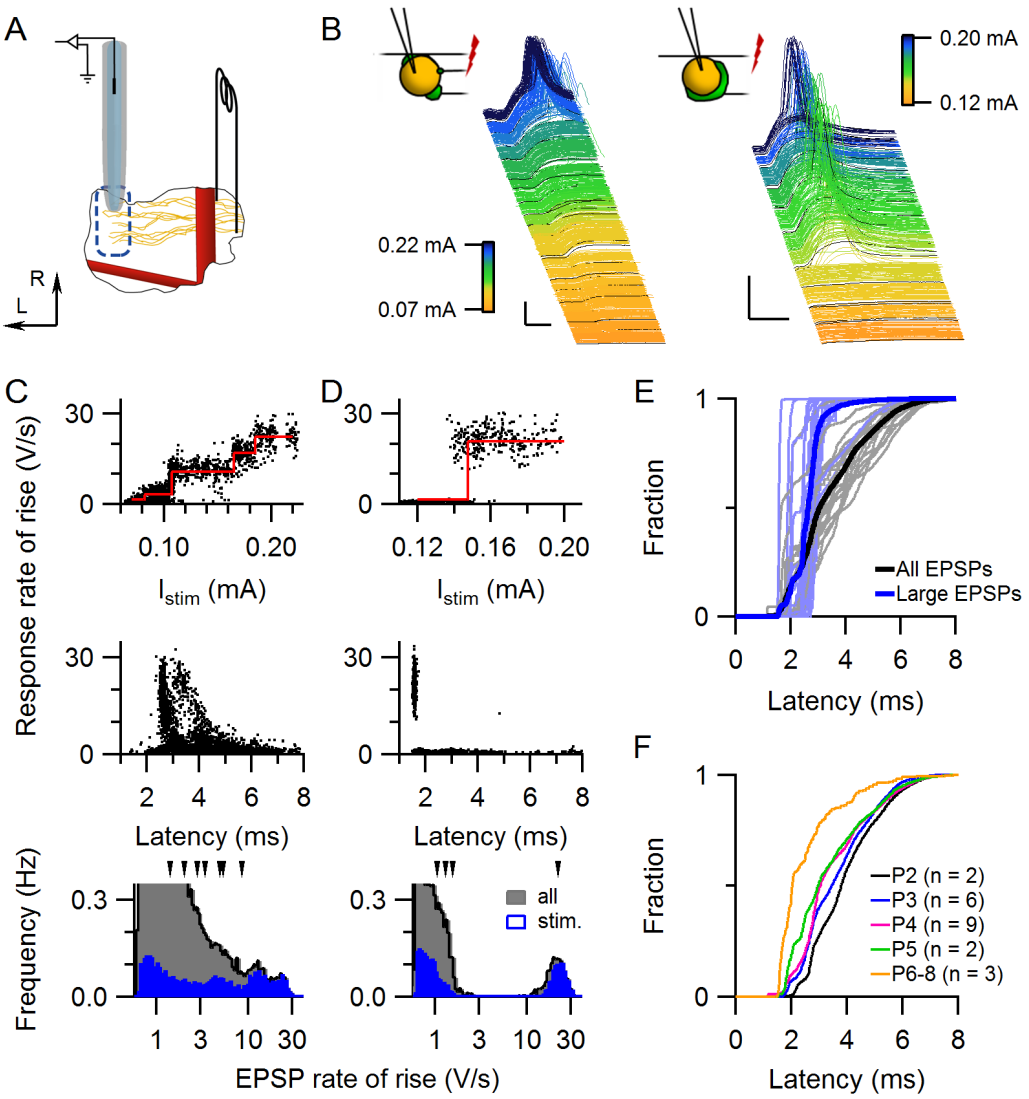


**Figure 1. Responses to current stimulation of developing calycigenic axons.** (A) Schematic drawing of the experimental approach. A bipolar stimulation electrode straddling the trapezoid body was positioned contralaterally from the recorded MNTB, and whole-cell recordings were made from principal cells of the MNTB. The basilar artery (rostrocaudal, thick red line) and the anterior-inferior cerebellar artery (mediolateral, red line) served as landmarks. Arrows indicate lateral (L) and rostral (R) directions. (B) Waterfall plots of two whole-cell recordings, sorted on stimulation intensity (color-coded as indicated in calibration bars). In the P4 example (left) a gradual increase in the evoked EPSP was observed, suggesting the recruitment of multiple inputs, while in the P6 example (right) a single, large EPSP was observed, which elicited a postsynaptic AP. Schematic drawing depicts the assumed

690 synaptic innervation. Scale bars indicate 25 mV and 2 ms. (C) Identification of synaptic inputs. Rates
691 of rise of evoked EPSPs vs. stimulation intensity (top) or EPSP latency (middle) for the P4 example
692 shown in B. The bottom graph shows the histograms of the rates of rise of evoked and spontaneous
693 EPSPs. Arrow heads on top of the graph indicate the rates of rise of identified inputs. Data points in
694 the top graph were horizontally scattered by <50 µA for visualization purposes. (D) As C, except for
695 the P6 example shown in B. (E) Cumulative distribution of latencies of all evoked EPSPs (black) and of
696 large EPSPs (>10 V/s, blue). Individual cells are shown in light blue and grey. Large EPSPs have a
697 shorter latency than most other EPSPs. (F) The average cumulative distribution of the evoked EPSP
698 latencies grouped by age suggests a developmental increase in propagation speed.

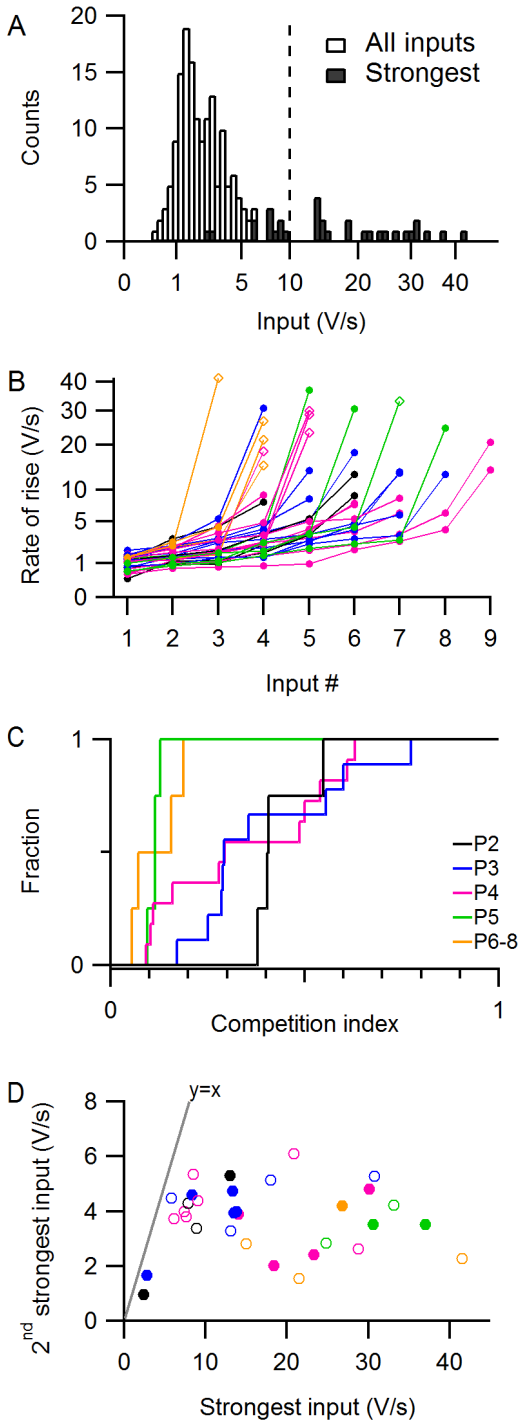


699 **Figure 2. Synaptic competition in MNTB follows the expansion of the strongest input without**

700 **changing the second strongest input.** (A) Histogram of the average rate of rise for all inputs (open)

701 and the strongest inputs (closed). Line indicates the threshold for 'strong inputs'. (B) For every cell

702 the inputs are incrementally sorted by their average EPSP rate of rise. Diamonds indicate the inputs

703 associated with a prespike. Colors indicate the ages as in C. Note the root scale of the ordinate. (C)
704 Cumulative distributions of the competition index, i.e. the ratio of the rates of rise of the second
705 strongest to the strongest input. (D) The rate of rise of the second strongest input against the
706 strongest. Markers correspond to individual principal cells. Closed markers indicate that both inputs
707 were identified based on spontaneous activity. Line shows identity line. Colors indicate age as in C.

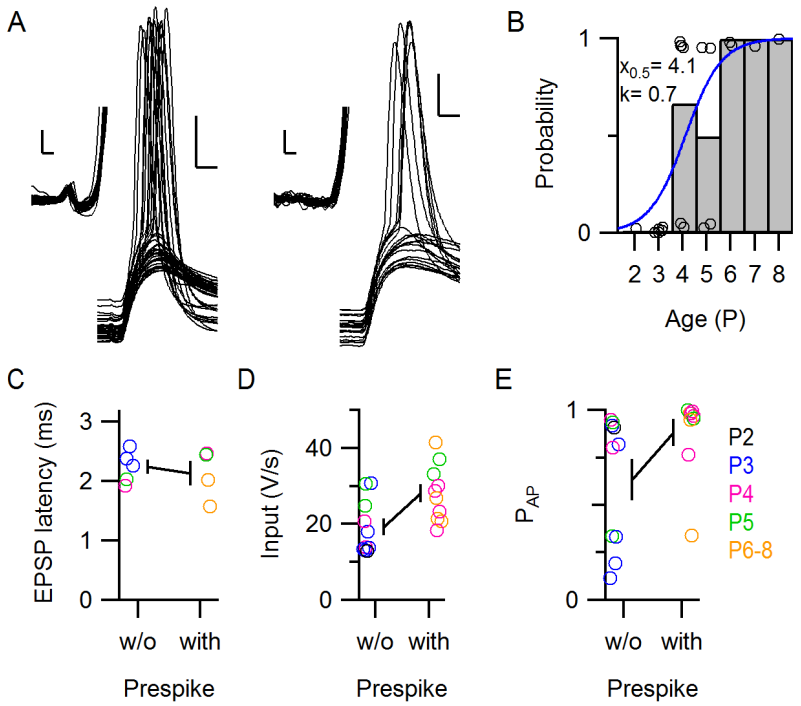


708 **Figure 3. Comparison of strong inputs with and without prespikes.** (A) Large EPSPs of a strong input
709 with (left; P6) and of a strong input without (right; P5) a prespike. EPSPs were aligned on their onset.
710 The insets show the same traces with their $V_m$ offsets subtracted. Scale bars indicate 10 mV and 1
711 ms, and scale bars in the inset indicate 0.5 mV and 0.2 ms. (B) Developmental changes in the
712 presence of a prespike preceding a large EPSP. Circles indicate cells where a large EPSP was
713 recorded. Bars represent age average. Blue line represents the fit of the logistic function with the
714 values reported in the graph. (C-E) Comparison of strong inputs with or without a prespike. In C only
715 evoked large EPSPs were analyzed. Circles indicate individual cells. Line represents the average and
716 SEM.

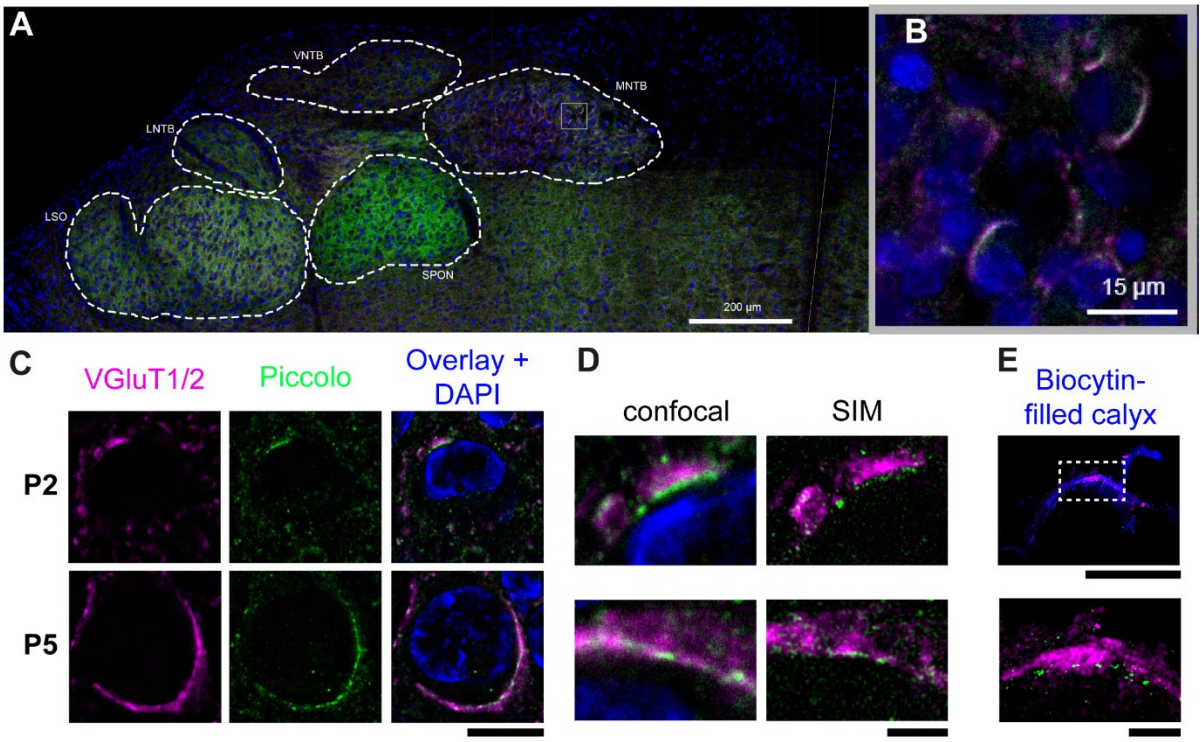


**Figure 4. Developmental expression of Piccolo in the MNTB.** (A) Fluorescent labeling of Piccolo (green), VGluT (magenta) and DAPI (blue) in the SOC of a P4 rat. Midline is indicated with a white line. Auditory nuclei are delineated with dashed lines. (B) Higher magnification of the grey box in A showing principal cells of the MNTB with large perisomatic clusters of VGluT and Piccolo. (C) A P2 and P5 principal cell with fluorescent labeling of VGluT, Piccolo, and VGluT + Piccolo + DAPI with confocal microscopy. (D) Comparison of confocal microscopy and structured-illumination microscopy (SIM) of perisomatic clusters of Piccolo and VGluT of the P2 principal cell shown in C (top), and of the P5 principal cell shown in C (bottom). (E) SIM image of a P5 biocytin-filled calyx (top, blue) with VGluT and Piccolo, revealing active zone-like structures in the Piccolo labeling (bottom). Non-calyceal labeling was masked. Scale bars indicate 200 µm in A, 15 µm in B, 10 µm in C, 2 µm in D, and 10 and 1 µm in E. Images in C and D were background-subtracted. Abbreviations: LSO, lateral superior olive; MNTB, medial nucleus of the trapezoid body; P, postnatal; SIM, structured-illumination microscopy; SOC, superior olivary complex; SPON, superior periolivary nucleus; VGluT, vesicular glutamate transporter 1 and 2; VNTB, ventral nucleus of the trapezoid body.

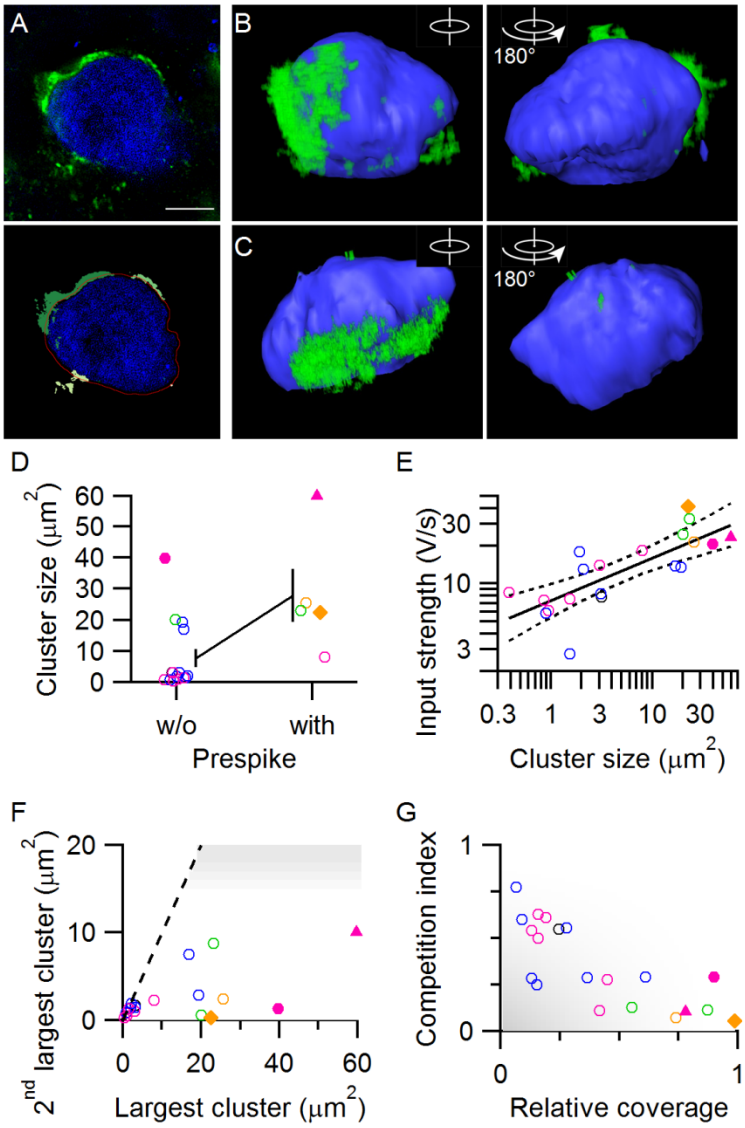


732 **Figure 5. Contact area of perisomatic VGluT clusters correlates with synaptic strength *in vivo*.** (A)
733 Example of segmentation of VGluT clusters around the soma. The image before (top) and after
734 segmentation (below). Blue: biocytin; Green: VGluT labeling. In the bottom image different VGluT
735 clusters are depicted by different shades of green. Red line indicates contour of the cell after
736 dilation. For this cell 1 input was associated with a prespike. (B-C) 3D reconstructions of somata
737 (blue) with VGluT clusters (green). Dendrites were manually removed. Right image is the same soma
738 after 180 degrees rotation. Postsynaptic cell in B did not have a prespike-associated input. The VGluT
739 cluster in C was manually separated from a nearby cluster that terminated on another cell. (D)

740 Largest VGluT cluster against the presence of a prespike-associated input. (E) Input strength of
741 strongest input against contact area of the largest VGluT cluster for each cell. Line indicates linear fit
742 of log-transformed variables. Dotted line indicates 95% confidence intervals. (F) Relation between
743 area of largest and second largest VGluT cluster. Shaded area: possibly multi-calyceal innervation.
744 (G) Competition index against relative coverage. Competition index equals the second strongest
745 input relative to the strongest input. Relative coverage equals the contact area of the largest VGluT
746 cluster relative to the total area contacted by VGluT clusters. Shaded area indicates region with low
747 competition index and low relative coverage. Colors in D-G indicate age as in previous figures.
748 Triangle indicates the data point that corresponds to the cell shown in A. Closed circle and diamond
749 indicate data points corresponding to the cells shown in B and C, respectively.